Combining fMRI and DTI: a framework for exploring the limits of fMRI-guided DTI fiber tracking and for verifying DTI-based fiber tractography results

Staempfli, P ; Reischauer, C ; Jaermann, T ; Valavanis, A ; Kollias, S ; Boesiger, P

DOI: https://doi.org/10.1016/j.neuroimage.2007.08.025

ELSEVIER

NeuroImage

www.elsevier.com/locate/ynimg
NeuroImage 39 (2008) 119–126

Combining fMRI and DTI: A framework for exploring the limits of fMRI-guided DTI fiber tracking and for verifying DTI-based fiber tractography results

P. Staempfli,[a,b,*] C. Reischauer,[a,1] T. Jaermann,[a] A. Valavanis,[b] S. Kollias,[b] and P. Boesiger[a]

[a]*Institute for Biomedical Engineering, ETH and University Zurich, Zurich, Switzerland*
[b]*Institute of Neuroradiology, University Hospital Zurich, Zurich, Switzerland*

Received 5 December 2006; revised 8 August 2007; accepted 20 August 2007
Available online 28 August 2007

A powerful, non-invasive technique for estimating and visualizing white matter tracts in the human brain *in vivo* is white matter fiber tractography that uses magnetic resonance diffusion tensor imaging. The success of this method depends strongly on the capability of the applied tracking algorithm and the quality of the underlying data set. However, DTI-based fiber tractography still lacks standardized validation. In the present work, a combined fMRI/DTI study was performed, both to develop a setup for verifying fiber tracking results using fMRI-derived functional connections and to explore the limitations of fMRI based DTI fiber tracking. Therefore, a minor fiber bundle that features several fiber crossings and intersections was examined: The striatum and its connections to the primary motor cortex were examined by using two approaches to derive the somatotopic organization of the striatum. First, an fMRI-based somatotopic map of the striatum was reconstructed, based on fMRI activations that were provoked by unilateral motor tasks. Second, fMRI-guided DTI fiber tracking was performed to generate DTI-based somatotopic maps, using a standard line propagation and an advanced fast marching algorithm. The results show that the fiber connections reconstructed by the advanced fast marching algorithm are in good agreement with known anatomy, and that the DTI-revealed somatotopy is similar to the fMRI somatotopy. Furthermore, the study illustrates that the combination of fMRI with DTI can supply additional information in order to choose reasonable seed regions for generating functionally relevant networks and to validate reconstructed fibers.

Introduction

Diffusion tensor imaging (DTI) (Basser et al., 1994; Pierpaoli et al., 1996) is a Magnetic Resonance Imaging (MRI) technique which allows us to measure the three dimensional (3D) Brownian motion of water molecules in the living human brain. In this fashion, the orientation of nerve fibers can be probed indirectly because water molecules diffuse preferentially parallel to the axonal fibers rather than perpendicular to them. The diffusion properties within each voxel are characterized by a symmetric diffusion tensor, whose principle eigenvector indicates the 3D orientation of the underlying fiber structure.

Fiber tracking allows for the virtual reconstruction of axonal networks within the brain on the basis of DTI data (for a review, see Mori and van Zijl, 2002). A variety of different tracking algorithms have been proposed; however, no standard procedure to quantify or to validate tracking results has been established so far. A key obstacle of fiber tractography is the uncertainty of the main diffusion direction. Due to the fact that the principal eigenvector does not correspond to the main fiber orientation in some instances, false trajectories may occur (Basser et al., 2000; Jones, 2003; Watts et al., 2003). In brain voxels with fiber crossing, branching, kissing, or merging, the tensor's principle eigenvector aligns along the averaged diffusion direction, and therefore, may not serve directly as a basis for fiber reconstruction. Furthermore, the tensors (and consequently the reconstructed fiber trajectories) can be compromised by partial volume effects or noise (Lazar and Alexander, 2003, 2005; Tournier et al., 2002). If the tracking algorithm incorporates solely the principal eigenvector for propagation, erroneous fiber pathways may be reconstructed. These obstacles have been addressed by recent studies. Many groups have proposed sophisticated techniques to improve fiber tracking (Lazar et al., 2003; Staempfli et al., 2006; Weinstein et al., 1999; Westin et al., 2002; Zhang et al., 2004).

A crucial input parameter for fiber tracking is the definition of an appropriate seed region. If seed areas are slightly changed by

* Corresponding author. Institute for Biomedical Engineering, University and ETH Zurich, Gloriastrasse 35, CH-8092 Zurich, Switzerland. Fax: +41 44 632 11 93.
E-mail address: staempfli@biomed.ee.ethz.ch (P. Staempfli).
[1] First and second author both contributed equally to this study.
Available online on ScienceDirect (www.sciencedirect.com).

1053-8119/$ - see front matter © 2007 Elsevier Inc. All rights reserved.
doi:10.1016/j.neuroimage.2007.08.025

only a few voxels, completely different fiber trajectories may be reconstructed. Also, large intersubject anatomical variations often exist, making it difficult to reliably define tracking seed areas based on anatomical landmarks. The complexity of the situation is increased when considering not only healthy volunteers but also patients suffering from space-occupying pathological processes (e.g., tumors). Different studies have attempted to solve this obstacle by combining DTI with fMRI. Thereby, start regions are defined in anatomical areas which are revealed by functional MRI (fMRI) activation patterns (Guye et al., 2003; Hendler et al., 2003; Watts et al., 2003). This combined approach may become clinically relevant for providing improved treatment planning information and patient outcome (Mori et al., 2002; Pamar et al., 2004; Staempfli et al., 2004).

In the present work, the main focus was to investigate a part of the motor system with a combination of DTI and fMRI. Known cortico-subcortical connections between the striatum and the primary motor cortex (PriMC) were examined. These connections have already been studied in primates in the early forties by Dusser et al. (Dusser de Barenne et al., 1942). They investigated projections from PriMC and sensory motor cortex to the putamen and the caudate nucleus. Kunzle et al. (Kunzle, 1975) performed an autoradiographic study and showed that the putamen is a major target of bilateral projections from the PriMC. Alexander et al. (Alexander and DeLong, 1985) stimulated single neuron cells within the basal ganglia which induced discrete movements of different body parts. A superio-inferior somatotopic gradient was found with face lying inferiorly, foot superiorly, and hand representation in between. Both studies concluded that the primate putamen is more directly involved in motor functions, whereas the caudate nucleus is involved in more complex behavioral functions.

In humans, two studies (Lehericy et al., 2004a,b) used fiber tractography to provide evidence that cortico-striatal connections are organized in discrete circuits, as in a monkey brain. However, the respective functions of these loops are still a matter of debate. The principal striatal circuit that is involved in the control of motor functions connects the cerebral cortex with the basal ganglia in a feedback loop. Fibers emerging from the motor cortex run along the internal and external capsule, respectively, and finally project in a somatotopic fashion upon the sensorimotor striatal territory (Nieuwenhuys et al., 1988). This is an area mainly within the superio-lateral sector of the postcommissural portion of the putamen. Several groups performed fMRI studies using different motor paradigms to asses this *in vivo* somatotopy of the basal ganglia (Gerardin et al., 2003; Lehericy et al., 1998; Maillard et al., 2000; Scholz et al., 2000). All studies showed a similar superio-inferior gradient of the foot, hand, and face representation within the putamen.

The two main goals of the present study were: (a) to derive a framework for verifying the results of DTI fiber tracking algorithms, and (b) to explore the limitations of fMRI-guided DTI fiber tracking. Therefore, known cortico-subcortical connections were reconstructed and investigated by deriving the somatotopic gradient in the putamen, twice. First, fMRI-based somatotopic maps were generated, using unilateral motor tasks. Second, DTI somatotopic maps were calculated, based on connection probabilities between striatal voxels and fMRI activations in the PriMC using two different DTI tracking algorithms. The resulting somatotopic maps were then compared and analyzed.

Materials and methods

Subjects

Twelve healthy, right-handed volunteers were scanned. Each subject gave informed written consent. Six of them were excluded after fMRI data analysis (see sub-section *Sites of activation* in the **Results** section). Of the resulting six volunteers two were female and four male (mean age 26.5±3.8 years). To test the handedness, the Edinburgh handedness inventory (Oldfield, 1971) was used. The subjects achieved values between 73.3 and 100, with a mean of 88.0±8.6.

Data acquisition

For data acquisition, a 3 T whole body MR system (Philips Achieva, Best, the Netherlands), equipped with 80 mT/m/ms gradient coils and an 8-element receive head coil array (MRI Devices Corp., Waukesha, USA), was used. Each imaging session consisted of a DTI scan, a high resolution T_1-weighted anatomical scan, and three fMRI scans using different motor paradigms. The field of view for all scans was defined as 200×200 mm^2, and the total scan time, including survey and sensitivity encoding reference scan, added up to 54 min.

For the DTI series, a whole brain diffusion-weighted single-shot spin-echo EPI sequence was applied with the following parameters: in-plane matrix=96×96, reconstructed to 128×128, 60 contiguous slices, slice thickness=2.1 mm, TE=50 ms, number of signal averages=2, 60% partial *k*-space acquisition. Diffusion weighting with a maximal *b*-factor of 1000 s/mm^2 was carried out along 15 icosahedral directions (Batchelor et al., 2003), complemented by one scan with $b=0$. Moreover, a 2.1-fold SENSE reduction factor (Pruessmann et al., 1999) was applied in order to reduce susceptibility artifacts and to enhance image quality (Bammer et al., 2002; Jaermann et al., 2004).

Anatomical data were obtained with a T_1-weighted TFE scan consisting of 180 contiguous slices (slice thickness=0.7 mm, in plane resolution=0.78×0.78 mm^2, TR=20 ms, $\alpha=20°$).

For the fMRI experiments, a gradient-echo EPI sequence, consisting of 30 contiguous slices, each with a spatial resolution of $1.56\times1.56\times4.2$ mm^3, was performed. The parameters were: TR=3000 ms, TE=40 ms, $\alpha=82°$, SENSE reduction factor=2.0. Each fMRI acquisition consisted of 7 blocks of 30 s motor activity alternating with 7 blocks of 30 s rest for a total time of 7 min.

Motor tasks

Three different motor tasks were used to create somatotopic maps of the PriMC and the striatum: (1) Foot task: Flexion and extension of the toes of the right foot with the ankle and proximal joints of the lower limb kept in a position of rest; (2) Hand task: Flexion and extension of the fingers of the right hand with the wrist and proximal joints of the upper limb kept in a position of rest; (3) Face task: Unilateral cheek movement, drawing the right angle of the mouth backwards and upwards. All experiments were practiced prior to scanning in order to achieve a constant performance of approximately ~1 Hz. The subjects were instructed to keep their eyes closed during the entire duration of the fMRI session. Start and stop instructions were given acoustically over earphones.

FMRI data analysis

The fMRI data were analyzed offline using SPM2 (SPM2; Wellcome Department of Cognitive Neurology, London, UK). After correcting the fMRI images for interscan motion artifacts, the data were analyzed both, without and with spatial normalization (using the SPM2 mean-EPI template). The first analysis was performed in order to enable the combination of fMRI and DTI data without prior spatial normalization of the DTI images, and the latter in order to achieve intersubject comparability for the fMRI-based somatotopic maps of the striatum. The images were smoothed with a Gaussian filter (kernel = 5 mm). A temporal cut-off of 128 s was applied to remove low frequency drift artifacts. Data from each run were then modeled, using the general linear model with separate, delayed boxcar functions. Multiple comparison correction was performed ($p < 0.05$) using the false discovery rate (FDR) method (Genovese et al., 2002). In the resulting SPM{t} maps, a threshold of 4 connected voxels was defined as minimal size for a significant cluster. Finally, the anatomical scans on which the left striatum was manually segmented for each subject were coregistered to the SPM{t} maps, whereas the spatial resolution of the SPM{t} maps was artificially increased to the resolution of the anatomical data.

Activation patterns in the entire brain were identified, and the corresponding anatomical regions were determined. For the somatotopy derivation in the putamen and subsequent postprocessing steps, only subjects were considered which showed fMRI activation in the putamen in at least 2 out of the 3 motor tasks. For the calculation of the fMRI somatotopy, the normalized SPM{t} maps of all subjects fulfilling the fMRI inclusion criteria were added up in a binary way to find which clusters inside the putamen were commonly activated in several subjects.

DTI data analysis

A correlation-based 3D-affine registration algorithm was used to achieve retrospective interscan motion correction and a reduction of eddy current-induced image warping (Netsch and vanMuiswinkel, 2004). The independent elements of the diffusion tensors and their corresponding eigenvalues/eigenvectors, the fiber tracks, and the DTI-based somatotopy in the putamen were computed with the use of an in-house software package.

The somatotopic maps were generated with the advanced Fast Marching (aFM) algorithm (Staempfli et al., 2006). In contrast to line propagation algorithms, fast marching techniques are based on evolving a 3D wave front through a volume of interest. The rate at which the front expands is linked to the local diffusion tensor and its orientation to adjacent diffusion tensors. Until today, all proposed FM algorithms incorporate only the principal eigenvector of the diffusion tensor in their calculations. Therefore, these methods fail to reconstruct fiber tracks in crossing or kissing areas. The newly developed aFM algorithm proposed an advanced implementation of FM, combining the advantages of classical FM and the tensor deflection approach (Lazar et al., 2003). The aFM algorithm takes into account the entire information contained in the diffusion tensor. Thereby, every tensor is classified as prolate (linear), oblate (planar), or spherical ellipsoid (Westin et al., 2002, 1997). During the actual tracking process, different adapted speed functions are applied for the front propagation, according to the shape classification of two adjacent voxels. As a result, the aFM algorithm features the capability to accurately evaluate brain areas containing fiber crossings and branching. An extensive algorithmic description of the basic fast marching technique can be found elsewhere (Parker et al., 2002a,b).

For each subject, the left striatum was manually segmented using T_1-weighted anatomical images which were coregistered to the DTI data beforehand. The seed regions for the tracking process were defined on the basis of the COGs of activations in the left precentral gyrus, obtained from the foot, hand, and face motor fMRI experiments. In order to be able to start the tracking algorithm in the adjacent white matter, the COGs were enlarged spherically. Thereby, all adjacent voxels whose midpoints were less than 3 mm away from the COG were included, resulting in a volume of 19 voxels (Staempfli et al., 2004). Due to the low anisotropy inside the striatum and within the starting regions in the precentral gyrus (Table 1), the tracking algorithm's fractional anisotropy stop criterion was decreased from 0.2 to a value of 0.1 in these areas.

Subsequently, tracking was initiated and performed thrice for every putamen voxel, starting from the left primary motor areas for foot, hand, and face representation, respectively. Then, each putamen voxel was colored according to the most likely (see section *Likelihood of connections*) of the three connections to the PriMC, yellow in case of a connection most likely to the face area, red to the foot, and green to the hand area. In the last step, the individual somatotopic DTI derived connectivity maps were spatially normalized, using SPM2 to identify regions commonly connected to the same cortical area within several subjects, equivalent to the analysis of the fMRI data. At the end, a visual analysis was performed to compare the fMRI and the DTI derived somatotopies. Additionally, for a more quantitative comparison, the percentage of the fMRI voxels (activated in four out of six subjects) that were correctly classified by the DTI-based somatotopy within the putamen was derived.

For comparison, somatotopic maps were generated using a common line propagation algorithm called "fiber assignment by continuous tracking" (FACT) (Mori and van Zijl, 2002). Finally, different cortico-striatal connections revealed by the FACT and the aFM algorithm were investigated and compared to known functional neuroanatomy.

Likelihood of connections

In the PriMC, three connections (i.e., from the foot, hand, and face regions) to every single voxel within the putamen were calculated. In order to assign a likelihood to each of the three estimated fiber trajectories, and thus, to choose the most probable connected cortical region for each voxel, a criterion for the likelihood of the connections was established. This approach compares the three differently evolved 3D wave fronts, as simulated by the aFM algorithm during the tracking process, which connect the cortical regions for foot, hand, and face representation with a specific voxel in the putamen. The principle idea is that the

Table 1

	Striatum	Face area	Foot area	Hand area
FA index	0.204±0.096	0.125±0.047	0.086±0.025	0.145±0.067
Number of voxels	1912±112	19	19	19

Mean values of the FA index inside the striatum as well as inside the spherical target regions for face, foot, and hand representation, averaged over the six subjects.

maximization of the surface of the 3D wave front, with respect to its volume, should reflect a more distinct diffusion behavior. In other words, in the case of isotropic diffusion, which reflects no inherent directional information, the wave front evolves spherically, resulting in a minimal surface and thus, a maximal volume to surface ratio (i.e., the higher the index, the lower the connection probability). A fundamental property of the likelihood criterion is its independence from the length of the fiber. Therewith the calculation of the LikelihoodIndex is not affected by the different distances of the cortical regions to the putamen which are induced by the underlying anatomy.

The ratio is given by:

$$\text{LikelihoodIndex} = \frac{\text{NumberofVolumeUnits}}{\text{NumberofSurfaceUnits} + 2 \cdot \text{NumberofVolumeUnits} - 2}$$

Thereby the NumberOfVolumeUnits defines the volume of the evolved 3D wave front at the time when the putamen voxel is reached. It is weighted with the NumberOfSurfaceUnits, which is a measure for the surface of the corresponding wave front. The other terms in the denominator arise from the requirement of making the ratio independent of the length of the fiber and are derived from the specifics of the applied aFM algorithm. For example in order to assign the same LikelihoodIndex to two similar fibers with different lengths, e.g., two straight fibers, one running over 5 voxels, the other over 10 voxels, the LikelihoodIndex would be

$$\frac{5}{22 + 2 \cdot 5 - 2} = \frac{10}{42 + 2 \cdot 10 - 2} = \frac{1}{6}.$$

Results

Sites of activation

In all subjects, activation in the left PriMC was elicited by all tasks. Furthermore, the fMRI analysis revealed activated clusters for at least two of the three motor tasks in 6 out of the 12 subjects within the putamen (five subjects for the foot and hand task, six subjects for the face task). Only the data of these six subjects were considered in further postprocessing steps.

Segmentation and localization of the striatum

In Fig. 1, a schematical depiction of the exact location of the left striatum, consisting of caudate nucleus and putamen, is presented on a high-resolution T1-map. Such 3D segmented areas were used to determine fMRI activations within the putamen and to define the striatal target regions for the tracking algorithms.

FMRI-based somatotopy

The fMRI analysis in the left putamen is depicted in Fig. 2. Fig. 2a reveals areas that were commonly activated in at least four out of the six subjects, whereas Fig. 2b depicts regions commonly activated in at least five out of the six subjects. It should be noted that these areas lie all within the sensorimotor putamen. The data in Fig. 2a show a superio-inferior gradient with face activation lying inferiorly, foot superiorly and hand in between. Furthermore, activation follows an anterio-posterior pattern, with face representation lying anteriorly, foot representation posteriorly, and hand in between. The two black arrows indicate the two gradients. However, Fig. 2b shows that these areas are strongly reduced when the activated areas that are common in at least five subjects are examined. However, the superio-inferior gradient is still apparent, indicated by the black arrow in Fig. 2b.

DTI-based somatotopy

In Fig. 3, the somatotopic map, generated from the spatially normalized single subject DTI derived connectivity maps, is shown. Areas within the putamen that are connected to the same PriMC area in multiple subjects are color-coded. Green voxels represent regions that are most likely connected to the hand area in at least five out of six subjects, red voxels represent regions most likely connected to the foot area in at least four out of six subjects and yellow voxels represent regions most likely connected to the face area in at least four out of six subjects. Different parameters were used because only a small number of voxels inside the putamen were commonly connected to the cortical face or foot region in five out of six subjects. White voxels stand for overlapping regions which result from the interpolation process during the spatial normalization of the individual somatotopic DTI derived connectivity maps.

The DTI-based somatotopic map in Fig. 3 shows an anterio-posterior gradient, indicated by the black arrow, similar to the one resulting from the fMRI data analysis (Fig. 2), with the face lying anteriorly, the foot posteriorly, and the hand in between. Contrary to the fMRI results, the superio-inferior gradient could not be reproduced. Additionally, it should be noted that clusters in the DTI somatotopy are also present in the anterior part of the putamen.

The calculation of a somatotopic map with the FACT algorithm was not possible since no connections between cortex and putamen

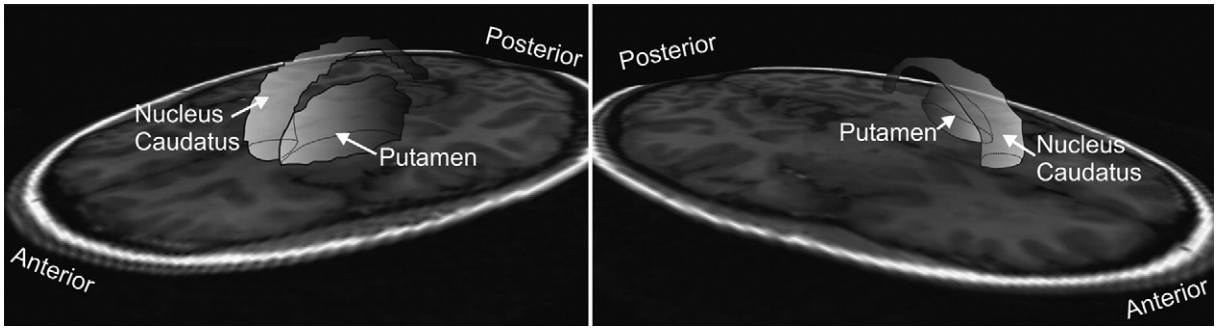

Fig. 1. Schematical depiction of the left striatum (medial and lateral view) on a high resolution T1 map. Highlighted are the caudate nucleus and the putamen.

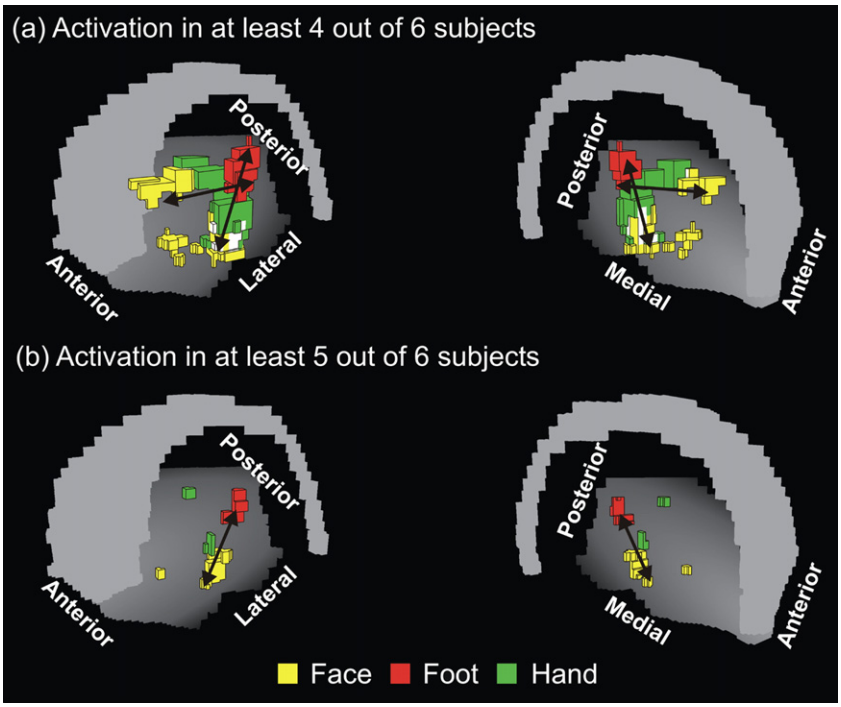

Fig. 2. Two lateral and medial views of the left striatum. Both figures show the 3D somatotopic group maps within the putamen, based on the fMRI BOLD contrast inside the putamen. Yellow voxels corresponds to face, red to foot, and green to hand movement. In (a) activation in at least four out of six subjects is depicted, whereas in (b) activation in at least five out of six subjects is shown. The anterio-posterior and the superio-inferior somatotopic gradient of face, foot, and hand representation are indicated by the black arrows.

could be established. Fiber analysis revealed that all fibers were deflected into several major fiber pathways, depending on the start location within the PriMC. Fibers that started in the foot and hand region mainly followed either the commissural system of the Corpus Callosum or the projectional cortico-spinal tracts, whereas fibers that started in the face area primarily followed short and long association fiber systems, establishing cortico-cortical connections. However, using the aFM algorithm, it was possible to reconstruct fibers that established connections between areas of the PriMC and the putamen. An example of three connections from the foot, hand, and face motor area to the corresponding somatotopic area in the putamen of one subject is depicted in Fig. 4. Thereby, as target regions in the putamen, the three selected end-voxels were defined within the somatotopic representation of face, foot, and hand, respectively.

Trajectories run along the internal and the external capsule to the PriMC. The cortico-striatal fibers are in good agreement with non-human primate (Kunzle, 1975) and known human white matter anatomy, as described in Krieg (Krieg, 1960).

Discussion

DTI fiber tracking allows for the reconstruction of various trajectories. However, in most cases, there is no implicit quantification of the resulting fibers. Interpretation of the DTI data without *a priori* anatomical knowledge is hardly possible.

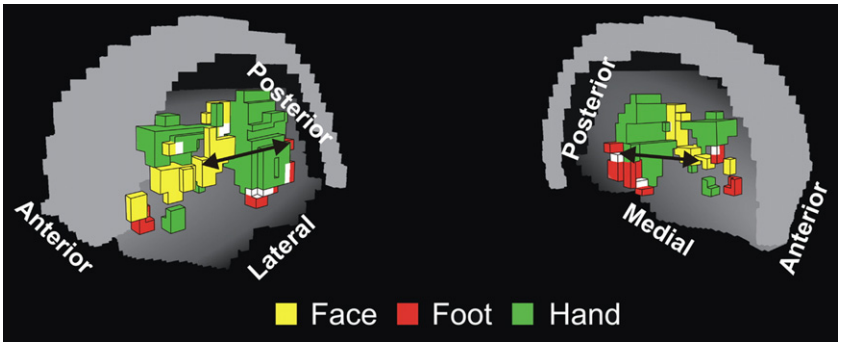

Fig. 3. The medial and lateral view of the left striatum is shown, depicting the DTI-based somatotopy within the putamen. Yellow voxels correspond to the face, red voxels to the foot, and green voxels to the hand area. The anterio-posterior somatotopic gradient of face, foot, and hand representation is indicated by the black arrows.

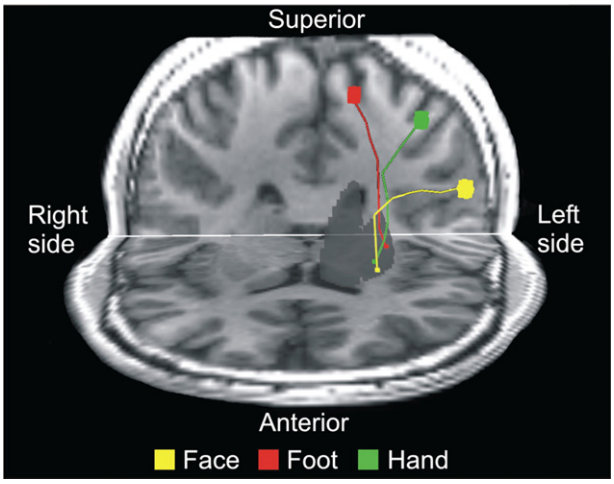

Fig. 4. Depiction of three exemplary reconstructed aFM fiber tracks between left PriMC and putamen in one subject. The fMRI cortex activations (yellow = face, red = foot, green = hand area) have been selected as seed regions. As target regions in the putamen, three voxels lying within the somatotopic representation of face, foot, and hand, respectively, were chosen.

Until today, no gold standard has been established for the verification of DTI-generated connection probabilities or DTI fiber tracks. In this study, the DTI data were complemented with information that was extracted from fMRI data for two reasons: (1) fMRI accurately defines functionally related structures that can be used as start and target regions for the tracking algorithms, which can be helpful in case of large anatomical variations (e.g., in the presence of a space occupying pathological disease), where it is almost impossible to define accurate tracking seed areas, based on common anatomical landmarks; (2) the fMRI-derived somatotopic map of the putamen served as a standard for comparing the somatotopic map generated by the DTI data. The main goal was to investigate if the known somatotopic gradient within the putamen could be reproduced twice, using solely fMRI as well as fMRI-guided DTI fiber tracking. This approach also enables to evaluate and compare different fiber tracking algorithms *in vivo*.

FMRI somatotopy revealed two gradients: a superio-inferior as well as an anterio-posterior gradient. The superio-inferior gradient, with the face lying inferiorly, foot superiorly, and hand in between, is in good agreement with recent fMRI studies in humans (Gerardin et al., 2003; Lehericy et al., 1998; Scholz et al., 2000) and studies in non-human primates (Alexander and DeLong, 1985; Flaherty and Graybiel, 1991, 1993; Kunzle, 1975; Liles and Updyke, 1985). The anterio-posterior gradient, with the face lying anteriorly, foot posteriorly, and hand in between, is contradictorily reported in literature (Gerardin et al., 2003; Kunzle, 1975; Maillard et al., 2000). However, a recently performed fMRI study by Gerardin et al. (Gerardin et al., 2003) shows results similar to the ones that are presented in this work. As already mentioned in a previous fMRI study (Scholz et al., 2000), it is difficult to find motor tasks which elicit consistent activation within the striatum. Thus, we had to exclude 6 out of 12 subjects after the fMRI analysis.

In the calculation of the DTI-based somatotopy, we refrained from choosing the entire fMRI-activated region in the PriMC as a seed area and established a more objective parameter based on the COGs of the activated regions in each individual subject. The individual extensions of the activated regions during specific tasks differed not only between subjects but also on an intrasubject basis when measurements were repeated, as also shown in (Liu et al., 2004; Tegeler et al., 1999; van Gelderen et al., 2005). Thus, the spherical seed region approach accounts for the individual functional neuroanatomy while providing comparable and reproducible start conditions between subjects. Furthermore, this approach was motivated by the dependence of fMRI results on the applied postprocessing steps (such as smoothing) and the statistical methods used for analysis which highly influence the size and the extension of fMRI activations.

The resulting DTI somatotopy, as revealed by the aFM algorithm, exhibits an anterio-posterior gradient similar to that of the fMRI-based somatotopy. However, the superio-inferior gradient in the DTI somatotopic map could not be reproduced in the present study. This is mainly due to the foot area in the DTI somatotopy being located more inferiorly than within the fMRI somatotopy. Visual comparison between the fMRI and DTI somatotopy reveals also that the different somatotopic areas of hand and face are not congruent but shifted by a few voxels against each other. This might be caused by the normalization and coregistration steps during data analysis, although it was taken care not to perform fiber tracking on normalized DTI data sets. A slight shift of the somatotopic clusters against each others results in a decrease of common overlapping areas. Therefore, it is not surprising that only 14.3% of the voxels in the hand area and 6.3% of the voxels in the face area overlap with the DTI revealed somatotopy. It should also be noted that only 12% of the voxels in the putamen were activated in the group fMRI somatotopic map. Furthermore, the hand area in the DTI somatotopy shows a larger representation in the putamen than the face and foot areas, which is physiologically expected. It should be noted, however, that five out of six subjects commonly exhibited a large representation of the hand area, whereas large areas of common face and foot representations were found in only four out of six subjects. It is hypothesized that this is most probably due to gray matter surrounding the cortical areas. Anisotropy in gray matter, and therefore, directional information, is strongly reduced. Thus, DTI fiber tracking within gray matter is generally less accurate and more prone to errors. In the present experiment, the expanding wave front of the aFM algorithm might evolve more isotropically from the face and foot area in the cortex, artificially decreasing the likelihood of the corresponding cortico-striatal connection. Furthermore, the hand area lies in prolongation of the cortico-spinal tract and may be favored more than the foot and face region. A better spatial resolution and higher sensitivity could increase tracking precision and avoid tracking errors due to missing directional diffusion information in gray matter. Additionally, different tracking start criteria might arise from the varying amount of included white matter voxels within the start regions, indicated by the FA values in the seed areas (see Table 1). FA values are the highest in the hand area, followed by those in the face and the foot region. Hence, the tracking procedure in the hand area might be accelerated, especially at the initial stage.

The implemented likelihood index allowed a ranking of different fiber connections relative to each other, according to an underlying model. The aim was to define a similar index as used in the fast marching publications by Parker et al. (Parker et al., 2002a,b) as well as in the advanced fast marching article by Staempli et al. (Staempfli et al., 2006). Therefore, the basic concepts of the index are closely related to the model of the applied fast marching tracking algorithm. The drawback of this approach is that this model does not allow the determination of absolute probabilities. Only relative probabilities between different fiber connections can be evaluated. However, an

absolute quantification of reconstructed fiber tracts is difficult to achieve since the establishment of a ground truth, e.g. by verification of reconstructed connections through histology or tracer techniques, would be the prerequisite for an absolute probabilistic index. In case of absolute quantification, the assignment of a probability value of 1 would mean that in reality a connection between a seed area and a target area is present exactly as reconstructed by the tracking algorithm. Correspondingly, a probability value of 0 would mean that no interconnection between two areas of interest exists. To the author's knowledge, presently no such absolute quantification of DTI fiber tracks exists.

As mentioned above, clusters within the DTI somatotopy in anterior areas of the putamen are present. However, as known from primate studies, this part functionally belongs to associative rather than motoric input (Parent and Hazrati, 1995). Thus, it is not surprising that no fMRI activation occurred in the corresponding area. One possibility for restricting the putamen region to only motoric input areas for DTI analysis would have been to use an fMRI mask containing all voxels activated by the three fMRI experiments. Due to the difficulty of eliciting fMRI activation within the putamen (Scholz et al., 2000), it might be possible that not all motoric input voxels showed fMRI evoked activation during the experiments. As a consequence, by using a joint fMRI mask to restrict the putamen area, one would risk to omit several motoric input voxels. Furthermore, by incorporating fMRI results of the putamen into the DTI evaluation, one would already presume that DTI and fMRI might produce similar somatotopic outputs. Thus, we refrained from subdividing or excluding any part of the putamen prior to DTI data analysis, due to the lack of sufficient information about the accurate functional division in the human putamen.

The potential of the aFM and the FACT tracking algorithms to reconstruct fibers spanning between cortex and putamen was explored with the purpose of evaluating their performance. While the aFM algorithm reconstructed both a clearly distinct somatotopy and fiber tracts that correspond to known anatomy, the standard FACT algorithm was unable to reconstruct any connection between cortex and putamen. Apparently, the FACT algorithm could not perform in the presence of the extensive fiber crossing that is known to occur in the centrum semiovale and particularly in the juxtacaudate area (Krieg, 1960). All trajectories were deflected by gross fiber bundles like the corpus callosum, the cortico-spinal tract or the long and short association fibers. However, another group (Lehericy et al., 2004a,b) was able to obtain cortico-striatal connections by using a similar line propagation algorithm that considered solely the direction of the first eigenvector.

In conclusion, the present study demonstrates that the combination of fMRI with DTI can supply additional information which may become clinically relevant, providing improved information for treatment planning and patient outcome. Even though the DTI and the fMRI somatotopy are not identical, the derived setup illustrates that fMRI-guided fiber tracking is a promising tool for addressing issues of functional connectivity in the human brain. FMRI provides the physiological information necessary to choose reasonable seed and target regions for the tracking algorithms, and the existence of the resulting fiber connections is complemented by their functional relationship. However, it has to be kept in mind that the relatively small cortico-striatal connections, unlike the major fiber pathways which they intersect, are difficult to reconstruct with DTI fiber tracking. In addition, fiber crossings and branchings that are encountered on the way from the PriMC to the putamen tested the boundaries of DTI fiber tractography. With this study, we clearly reached the limits of today's DTI fiber tracking technique. Hence, not surprisingly, the fMRI somatotopic map of the putamen is not congruent with the DTI somatotopic map which becomes also apparent quantitatively by the percentage of the overlapping fMRI and DTI somatotopic clusters, as described above. To further refine the setup developed in this study, one could implement and apply tracking algorithms which are based on diffusion data that resolve multiple fiber directions within one voxel. Thereby, higher order mathematical tensor models, as proposed in different studies (Frank, 2001, 2002; Tuch, 2004; Tuch et al., 2002, 2003), could provide a possible basis. These techniques are still restricted to scientific research due to long acquisition times and limited spatial resolution.

Furthermore, due to low anisotropy in gray matter, tracking has to be improved in the transition area of gray to white matter in order to more reliably merge information from fMRI and DTI data. This could be achieved by increasing both spatial resolution and diffusion sensitivity during data acquisition. Diffusion sensitivity, higher spatial resolution, and consequently an increase of data quality, especially for higher order tensor model data, will gain from the transition to higher static magnetic field strengths. Therefore, the developed technique holds great promise for improving the accuracy of quantification, comparison, and verification of fiber tracking algorithms and results.

Acknowledgments

The authors are grateful for the continuing support of Philips Medical Systems and for the financial support given by the Strategic Excellence Project Program (SEP) of the ETH Zurich.

References

Alexander, G.E., DeLong, M.R., 1985. Microstimulation of the primate neostriatum. II. Somatotopic organization of striatal microexcitable zones and their relation to neuronal response properties. J. Neurophysiol. 53, 1417–1430.

Bammer, R., Auer, M., Keeling, S.L., Augustin, M., Stables, L.A., Prokesch, R.W., Stollberger, R., Moseley, M.E., Fazekas, F., 2002. Diffusion tensor imaging using single-shot SENSE-EPI. Magn. Reson. Med. 48, 128–136.

Basser, P.J., Mattiello, J., LeBihan, D., 1994. MR diffusion tensor spectroscopy and imaging. Biophys. J. 66, 259–267.

Basser, P.J., Pajevic, S., Pierpaoli, C., Duda, J., Aldroubi, A., 2000. In vivo fiber tractography using DT-MRI data. Magn. Reson. Med. 44, 625–632.

Batchelor, P.G., Atkinson, D., Hill, D.L., Calamante, F., Connelly, A., 2003. Anisotropic noise propagation in diffusion tensor MRI sampling schemes. Magn. Reson. Med. 49, 1143–1151.

Dusser de Barenne, J., Garol, H., McCulloch, W., 1942. Physiological neuronography of the cortico-striatal connections. Res. Publ.-Assoc. Nerv. Ment. Dis. 21, 246–266.

Flaherty, A.W., Graybiel, A.M., 1991. Corticostriatal transformations in the primate somatosensory system. Projections from physiologically mapped body-part representations. J. Neurophysiol. 66, 1249–1263.

Flaherty, A.W., Graybiel, A.M., 1993. Two input systems for body representations in the primate striatal matrix: experimental evidence in the squirrel monkey. J. Neurosci. 13, 1120–1137.

Frank, L.R., 2001. Anisotropy in high angular resolution diffusion-weighted MRI. Magn. Reson. Med. 45, 935–939.

Frank, L.R., 2002. Characterization of anisotropy in high angular resolution diffusion-weighted MRI. Magn. Reson. Med. 47, 1083–1099.

Genovese, C.R., Lazar, N.A., Nichols, T., 2002. Thresholding of statistical

maps in functional neuroimaging using the false discovery rate. NeuroImage 15, 870–878.
Gerardin, E., Lehericy, S., Pochon, J.B., Tezenas du Montcel, S., Mangin, J.F., Poupon, F., Agid, Y., Le Bihan, D., Marsault, C., 2003. Foot, hand, face and eye representation in the human striatum. Cereb. Cortex 13, 162–169.
Guye, M., Parker, G.J., Symms, M., Boulby, P., Wheeler-Kingshott, C.A., Salek-Haddadi, A., Barker, G.J., Duncan, J.S., 2003. Combined functional MRI and tractography to demonstrate the connectivity of the human primary motor cortex in vivo. NeuroImage 19, 1349–1360.
Hendler, T., Pianka, P., Sigal, M., Kafri, M., Ben-Bashat, D., Constantini, S., Graif, M., Fried, I., Assaf, Y., 2003. "Two are Better than One": Combining fMRI and DTI Based Fiber Tracking for Effective Pre-Surgical Mapping. Proc. Int Soc Magn Reson Med, Toronto.
Jaermann, T., Crelier, G., Pruessmann, K.P., Golay, X., Netsch, T., van Muiswinkel, A.M., Mori, S., van Zijl, P.C., Valavanis, A., Kollias, S., et al., 2004. SENSE-DTI at 3 T. Magn. Reson. Med. 51, 230–236.
Jones, D.K., 2003. Determining and visualizing uncertainty in estimates of fiber orientation from diffusion tensor MRI. Magn. Reson. Med. 49, 7–12.
Krieg, W.J.S., 1960. Slice Reconstructions of Human Cerebral Sections. Brain Books, Evanston, IL.
Kunzle, H., 1975. Bilateral projections from precentral motor cortex to the putamen and other parts of the basal ganglia. An autoradiographic study in *Macaca fascicularis*. Brain Res. 88, 195–209.
Lazar, M., Alexander, A.L., 2003. An error analysis of white matter tractography methods: synthetic diffusion tensor field simulations. NeuroImage 20, 1140–1153.
Lazar, M., Alexander, A.L., 2005. Bootstrap white matter tractography (BOOT-TRAC). NeuroImage 24, 524–532.
Lazar, M., Weinstein, D.M., Tsuruda, J.S., Hasan, K.M., Arfanakis, K., Meyerand, M.E., Badie, B., Rowley, H.A., Haughton, V., Field, A., et al., 2003. White matter tractography using diffusion tensor deflection. Hum. Brain Mapp. 18, 306–321.
Lehericy, S., van de Moortele, P.F., Lobel, E., Paradis, A.L., Vidailhet, M., Frouin, V., Neveu, P., Agid, Y., Marsault, C., Le Bihan, D., 1998. Somatotopical organization of striatal activation during finger and toe movement: a 3-T functional magnetic resonance imaging study. Ann. Neurol. 44, 398–404.
Lehericy, S., Ducros, M., Krainik, A., Francois, C., Van de Moortele, P.F., Ugurbil, K., Kim, D.S., 2004a. 3-D diffusion tensor axonal tracking shows distinct SMA and pre-SMA projections to the human striatum. Cereb. Cortex 14, 1302–1309.
Lehericy, S., Ducros, M., Van de Moortele, P.F., Francois, C., Thivard, L., Poupon, C., Swindale, N., Ugurbil, K., Kim, D.S., 2004b. Diffusion tensor fiber tracking shows distinct corticostriatal circuits in humans. Ann. Neurol. 55, 522–529.
Liles, S.L., Updyke, B.V., 1985. Projection of the digit and wrist area of precentral gyrus to the putamen: relation between topography and physiological properties of neurons in the putamen. Brain Res. 339, 245–255.
Liu, J., Brown, R., Yue, G., 2004. Reproducibility of fMRI at 1.5 T in a strictly controlled motor task. Magn. Reson. Med. 52, 751–760.
Maillard, L., Ishii, K., Bushara, K., Waldvogel, D., Schulman, A.E., Hallett, M., 2000. Mapping the basal ganglia: fMRI evidence for somatotopic representation of face, hand, and foot. Neurology 55, 377–383.
Mori, S., van Zijl, P.C., 2002. Fiber tracking: principles and strategies—A technical review. NMR Biomed. 15, 468–480.
Mori, S., Frederiksen, K., van Zijl, P.C., Stieltjes, B., Kraut, M.A., Solaiyappan, M., Pomper, M.G., 2002. Brain white matter anatomy of tumor patients evaluated with diffusion tensor imaging. Ann. Neurol. 51, 377–380.
Netsch, T., vanMuiswinkel, A., 2004. Quantitative evaluation of image-based distortion correction in diffusion tensor imaging. IEEE Trans. Med. Imag. 23, 789–798.
Nieuwenhuys, R., Voogd, J., van Huijzen, C., 1988. The Human Central Nervous System. Spinger, Verlag.
Oldfield, R.C., 1971. The assessment and analysis of handedness: the Edinburgh inventory. Neuropsychologia 9, 97–113.
Pamar, H., Sitoh, Y., Yeo, T., 2004. Combined magnetic resonance tractography and functional magnetic resonance imaging in evaluation of brain tumors involving the motor system. J. Comput. Assist. Tomogr. 28, 551–556.
Parent, A., Hazrati, L.-N., 1995. Functional anatomy of the basal ganglia. I. The cortico-basal ganglia-thalamo-cortical loop. Brain Res. 20, 91–127.
Parker, G.J., Stephan, K.E., Barker, G.J., Rowe, J.B., MacManus, D.G., Wheeler-Kingshott, C.A., Ciccarelli, O., Passingham, R.E., Spinks, R.L., Lemon, R.N., et al., 2002a. Initial demonstration of in vivo tracing of axonal projections in the macaque brain and comparison with the human brain using diffusion tensor imaging and fast marching tractography. NeuroImage 15, 797–809.
Parker, G.J.M., Wheeler-Kingshott, C.A.M., Barker, G.J., 2002b. Estimating distributed anatomical connectivity using fast marching methods and diffusion tensor imaging. IEEE Trans. Med. Imag. 21, 505–512.
Pierpaoli, C., Jezzard, P., Basser, P.J., Barnett, A., Di Chiro, G., 1996. Diffusion tensor MR imaging of the human brain. Radiology 201, 637–648.
Pruessmann, K.P., Weiger, M., Scheidegger, M.B., Boesiger, P., 1999. SENSE: sensitivity encoding for fast MRI. Magn. Reson. Med. 42, 952–962.
Scholz, V.H., Flaherty, A.W., Kraft, E., Keltner, J.R., Kwong, K.K., Chen, Y.I., Rosen, B.R., Jenkins, B.G., 2000. Laterality, somatotopy and reproducibility of the basal ganglia and motor cortex during motor tasks. Brain Res. 879, 204–215.
Staempfli, P., Jaermann, T., Valavanis, A., Boesiger, P., Kollias, S., 2004. fMRI based fiber tracking using SENSE-DTI at 3 Tesla; 2004; Kyoto, Japan. p. 1287.
Staempfli, P., Jaermann, T., Crelier, G.R., Kollias, S., Valavanis, A., Boesiger, P., 2006. Resolving fiber crossing using advanced fast marching tractography based on diffusion tensor imaging. NeuroImage 30, 110–120.
Tegeler, C., Strother, S.C., Anderson, J.R., Kim, S.G., 1999. Reproducibility of BOLD-based functional MRI obtained at 4 T. Hum. Brain Mapp. 7, 267–283.
Tournier, J.D., Calamante, F., King, M.D., Gadian, D.G., Connelly, A., 2002. Limitations and requirements of diffusion tensor fiber tracking: an assessment using simulations. Magn. Reson. Med. 47, 701–708.
Tuch, D.S., 2004. Q-ball imaging. Magn. Reson. Med. 52, 1358–1372.
Tuch, D.S., Reese, T.G., Wiegell, M.R., Makris, N., Belliveau, J.W., Wedeen, V.J., 2002. High angular resolution diffusion imaging reveals intravoxel white matter fiber heterogeneity. Magn. Reson. Med. 48, 577–582.
Tuch, D.S., Reese, T.G., Wiegell, M.R., Wedeen, V.J., 2003. Diffusion MRI of complex neural architecture. Neuron 40, 885–895.
van Gelderen, P.C.W.H.W., de Zwart, J.A., Cohen, L., Hallett, M., Duyn, J.H., 2005. Resolution and reproducibility of BOLD and perfusion functional MRI at 3.0 Tesla. Magn. Reson. Med. 54, 569–576.
Watts, R., Liston, C., Niogi, S., Ulug, A.M., 2003. Fiber tracking using magnetic resonance diffusion tensor imaging and its applications to human brain development. Ment. Retard. Dev. Disabil. Res. Rev. 9, 168–177.
Weinstein, D., Kindlmann, G., Lundberg, E., 1999. Tensorlines: advection-diffusion based propagation through diffusion tensor fields. IEEE Vis. 249–253.
Westin, C.F., Peled, S., Gudbjartsson, H., Kikinis, R., Jolesz, F.A., 1997. Geometrical diffusion measures for MRI from tensor basis analysis. Proceedings of the 5th Annual Meeting of ISMRM, Vancouver, 1742.
Westin, C.F., Maier, S.E., Mamata, H., Nabavi, A., Jolesz, F.A., Kikinis, R., 2002. Processing and visualization for diffusion tensor MRI. Med. Image Anal. 6, 93–108.
Zhang, S., Bastin, M.E., Laidlaw, D.H., Sinha, S., Armitage, P.A., Deisboeck, T.S., 2004. Visualization and analysis of white matter structural asymmetry in diffusion tensor MRI data. Magn. Reson. Med. 51, 140–147.